Ecological Informatics 71 (2022) 101777

Contents lists available at ScienceDirect

Ecological Informatics

journal homepage: www.elsevier.com/locate/ecolinf

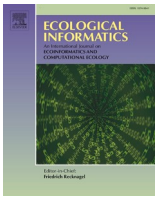

Modelling and evaluation of land use changes through satellite images in a multifunctional catchment: Social, economic and environmental implications

Carolina Acuña-Alonso [a,*], Ana Novo [b], Juan Luis Rodríguez [b], Simone Varandas [c], Xana Álvarez [a]

[a] Agroforestry Group, Department of Natural Resources and Environmental Engineering, School of Forestry Engineering, University of Vigo, 36005 Pontevedra, Spain
[b] Geotech-Group, CINTECX, Department of Natural Resources and Environmental Engineering, School of Mining Engineering, University of Vigo, 36310 Vigo, Spain
[c] CITAB-Inov4Agro – Centre for the Research and Technology of Agro-Environmental and Biological Sciences, University of Trás-os-Montes and Alto Douro, 5000-801 Vila Real, Portugal.

ARTICLE INFO

Keywords:
Nature-based solutions
Flood hazard management
Water Governance
Land-use change, Random Forest, HEC-HMS, Sentinel-2

ABSTRACT

Floods are recurrent phenomena with significant environmental and socio-economic impacts. The risk of flooding increases when land use changes. The objective of this research is to detect land cover changes via Sentinel-2 images in the Umia Basin (Galicia, NW Spain) in 2016–2021 and to analyse the associated flood risk. This study focuses on how forest use and nature-based solutions (NBS) can reduce the risk and hazard of flooding in cities and crops in the high-risk area. A flood simulation was performed with the land use obtained from Sentinel-2 (Observed) and three more simulations were performed changing the location of afforestation and NBS, i.e. "S-Upstream", "S-Downstream" and "S-Total". Finally, the environmental, economic and social impacts of the scenarios designed and estimated are analysed and discussed. Land cover change was successfully monitored with Sentinel-2 imagery. The catchment area showed noteworthy changes in land use, most notably for the category of trees, which covered 6700 ha in 2016 and 10,911 ha in 2021. However riparian vegetation decreased by almost 11%. For the flood hazard simulations, an average reduction in peak discharge was obtained for all three scenarios (9.3% for S-Up; 8.6% for S-Down and 13% for S-Total). From the economic perspective, all three scenarios show a positive net present value for the period studied. However, S-Down is the scenario with the lowest benefits (€15,476,487), while S-Up and S-Total show better values at €29,580,643 and €65,158,130 respectively. However, investment cost is much higher for the S-Total scenario, and upstream actions affect the whole catchment, so S-Up is the best decision. This study concludes that the information provided by satellites is a large-scale analysis tool for small heterogeneous plots that facilitates the comprehensive analysis of a territory. This information can be incorporated into flood analysis models, facilitating simulation through the use of NBS. It has been proven that the use of reforestation upstream only is almost as beneficial as reforestation in the entire catchment and is economically more viable. This confirms that the methodology used reduces flood hazard, despite the territorial complexity, facilitating decision making on the use of NBS.

1. Introduction

Land use and land cover (LULC) are important because increased urbanisation, industry and rural abandonment play important roles in local climate, hydro-geological conditions, floodplain biogeochemical processes and environmental sustainability (Nath et al., 2021). These changes consist mainly of logging and destruction of vegetation on forest land, e.g. destruction of riparian vegetation (Dewan and Yamaguchi, 2009). These degradation processes potentially lead to an increase in the percentage of impervious surface cover in the area, and thus to changes

Abbreviations: NBS, Nature-based solutions; LULC, Land use and land cover; HEC-HMS, Hydrologic Modelling System; RS, remote sensing; GIS, geographic information system; L1C, Level 1C; TOA, Top of atmosphere; L2A, Level 2A; BOA, Bottom of the atmosphere; DOS, Dark Object Subtraction; RF, Random Forest; PNOA, National Aerial Orthophotography Plan; SCS, Soil Conservation Service; CN, Curve Number; CBA, Cost-benefit analysis.

* Corresponding author.
E-mail addresses: carolina.alonso@uvigo.es (C. Acuña-Alonso), annovo@uvigo.es (A. Novo), jlsomoza@uvigo.es (J.L. Rodríguez), simonev@utad.pt (S. Varandas), xaalvarez@uvigo.es (X. Álvarez).

https://doi.org/10.1016/j.ecoinf.2022.101777
Received 21 June 2022; Received in revised form 1 August 2022; Accepted 13 August 2022
Available online 19 August 2022

in hydrodynamic framework and floodplain structures (McGrane, 2016). In addition, climate change has caused hydrological changes around the world, increasing the likelihood of extreme weather events such as floods (Rajkhowa and Sarma, 2021). LULC changes and increases in extreme weather events mean that ecosystems are not sufficiently resilient to these natural hazards (Avand et al., 2021). Therefore, such events can negatively affect ecosystems and communities, resulting in huge socio-economic impacts, destruction of infrastructure and environmental disruption (Chowdhuri et al., 2020).

In this context, the development of flood risk resilience governance policies needs to be increased. This will strengthen society's ability to prevent and mitigate flood risk through the implementation of adaptation tools in a changing climate scenario. Land use/land cover maps are an excellent tool for monitoring and managing natural resources, and can improve the development of strategies for adapting to climate change and its various impacts (Thanh Noi and Kappas, 2018). Such maps are key documents that provide information for various applications, such as land use policy development, ecosystem services, urban planning, conservation, agricultural monitoring and dynamic LULC assessment. Remote sensing is an essential tool for creating such land use maps over large areas. The setting up of the Copernicus Programme by the European Space Agency (ESA) and the European Union (EU) has contributed to the effective monitoring of the Earth's surface. The most significant contribution was the launch of multispectral imaging instruments (MSI) capable of recording 13 wide bands via the Sentinel-2 satellites Sentinel-2A (launched on 23 June 2015) and Sentinel-2B (launched on 7 March 2017). One of the essential applications for Sentinel-2 data is LULC monitoring (Bruzzone et al., 2017). This has become essential for decision making and management to assess the status of the Earth's surface, e.g. identification of tree species (Arasumani et al., 2021), water quality (Viso-Vázquez et al., 2021) and fire risk analysis (Novo et al., 2020).

Hydrological modelling is another tool with great potential in land management. Such models include the Hydrological Modelling System of the Centre for Hydrological Engineering and the Soil and Water Assessment Tool (SWAT) (Arnold et al., 1998), though the best known distributed hydrological models are that of the European Hydrological System (MIKE-SHE) (Refshaard and Storm, 1995) and the Modular Modelling System (MMS) (Leavesley et al., 1996). The Hydrologic Modelling System (HEC-HMS), a software app developed by the US Army Corps of Engineers Hydrologic Engineering Center (HEC), is a numerical, semi-distributed hydrologic model used for event-based and continuous runoff simulation (Ford et al., 2002).

On the practical application of both remote sensing and hydrological modelling, there have been many studies on land cover use classification which use Sentinel-2 images (Carrasco et al., 2019; Forkuor et al., 2018; Malinowski et al., 2020; Qiu et al., 2019; Sánchez-Espinosa and Schröder, 2019; Sekertekin et al., 2017; Weigand et al., 2020). The use of remote sensing (RS) and geographic information system (GIS) technologies for flood prediction, preparedness, prevention and risk assessment worldwide is presented as a state-of-the-art methodology (Zhang et al., 2019). There are also various studies that analyse flood risks and responses through hydrological models (Halwatura and Najim, 2013; Kalantari et al., 2015; Mattos et al., 2022). In addition, researchers have begun to use the coupled hydrological-hydraulic model for future floodplain mapping and for risk assessment in different parts of the world (Cowles, 2021). But currently, these two knowledge areas have not been combined to advance and improve land management and take advantage of potential synergies between them to improve decision-making by managers. Adopting hydrological models combined with GIS tools in a given area is always a challenge. In fact, the use of HEC-HMS is relatively low in Spain, and even more so in Galicia, where land use conflicts are high and where plot size is very small and characterised by smallholdings (average plot size is 0.26 ha). In other words, the application of RS from satellite images offers the opportunity to model responses to precipitation events with instantaneous real data, analyse responses in the past and predict future events and their impact. In addition, the resolution of these images (10 m) means that changes in land use can be detected with a considerable level of detail. Moreover, large-scale analysis can be included and the major technical, economic and resource efforts entailed by other, conventional methods can be avoided. Both tools could be used in the development of specific flood hazard management plans, river basin management plans or urban plans. These could address the current lack of knowledge on the implementation of preventive flood risk mitigation measures, such as the application of Nature-based solutions (NBS) (Brillinger et al., 2021). NBS are framed as an alternative approach for addressing current societal challenges that aims to work with nature rather than against it (Seddon et al., 2020). Some of these techniques involve the use of green infrastructure and natural water retention measures, such as land use conversion through afforestation to improve evapotranspiration, infiltration and retention of water, land management practices that help increase the water holding capacity of soils and the reconnection of floodplains or ponds to rivers (Collentine and Futter, 2018).

The study area proposed in this work is the hydrographic basin of the Umia River. This river has a reservoir built in 2000 with the dual objective of supplying drinking water to the population of the region and preventing repeated floods in the largest town in the area (Caldas de Reis). In past decades, the engineering solutions provided to address type of problem usually entailed the construction of transversal infrastructures that served to control the flow in strong precipitation events (Nakamura and Shimatani, 2021). But today, natural solutions such as NBS have been shown to complement or even successfully replace them (Vojinovic et al., 2021). In this way, the initial hypothesis is that the strategic application of NBS can reduce the risk of flooding in this study area and improve on the results of the solutions provided in past decades. Accordingly, based on a comprehensive land management approach, the study 1) analyses the potential of Sentinel-2 images for estimating LULC the changes in the very small plots on the Umia River basin (Galicia, northwest Spain) from 2016 to 2021; 2) analyses the impacts of those changes for flood hazard in cities and crops located in the high-risk area; 3) simulates possible scenarios of changes via afforestation and NBS to reduce the risk of this natural hazard; and 4) analyses and discusses the possible environmental, economic and social impacts of various scenarios. The innovation proposed in this study is the comprehensive management of river basins based on the use of satellites as large-scale analysis tools for defining, analysing and monitoring LULC changes. In addition, the potential impacts of those changes on the basin are considered and different scenarios are designed with the aim of reducing potential risks and quantifying their social, economic and environmental impacts. All this will help land management decision makers to do their job by providing better data, information and tools. Currently, these issues have been addressed separately, i.e. the different configurations and links have not been integrated into the same analysis. That is why this study represents an advance in the use and combination of different disciplines and tools for better water governance.

2. Materials and methods

2.1. Study area

The Umia Basin is in Pontevedra, in the southwest of Galicia, Spain (Fig. 1). The Umia River, which forms the central axis of this basin, has an area of 44,590 ha and flows for a total of 70 km with an average flow-rate of 16.3 m^3/s. The predominant climate in the study area is oceanic, with an average annual rainfall of 143.72 L/m^2 and an average temperature of 13.6 °C, in 2021. Accordingly, the period with the highest flow rates is between December and May, with the lowest being in August.

Like many other rivers in Europe, the Umia ecosystem has been affected by human activities such as land use change, agriculture, plantations and pastures. The Spanish Land Use Information System

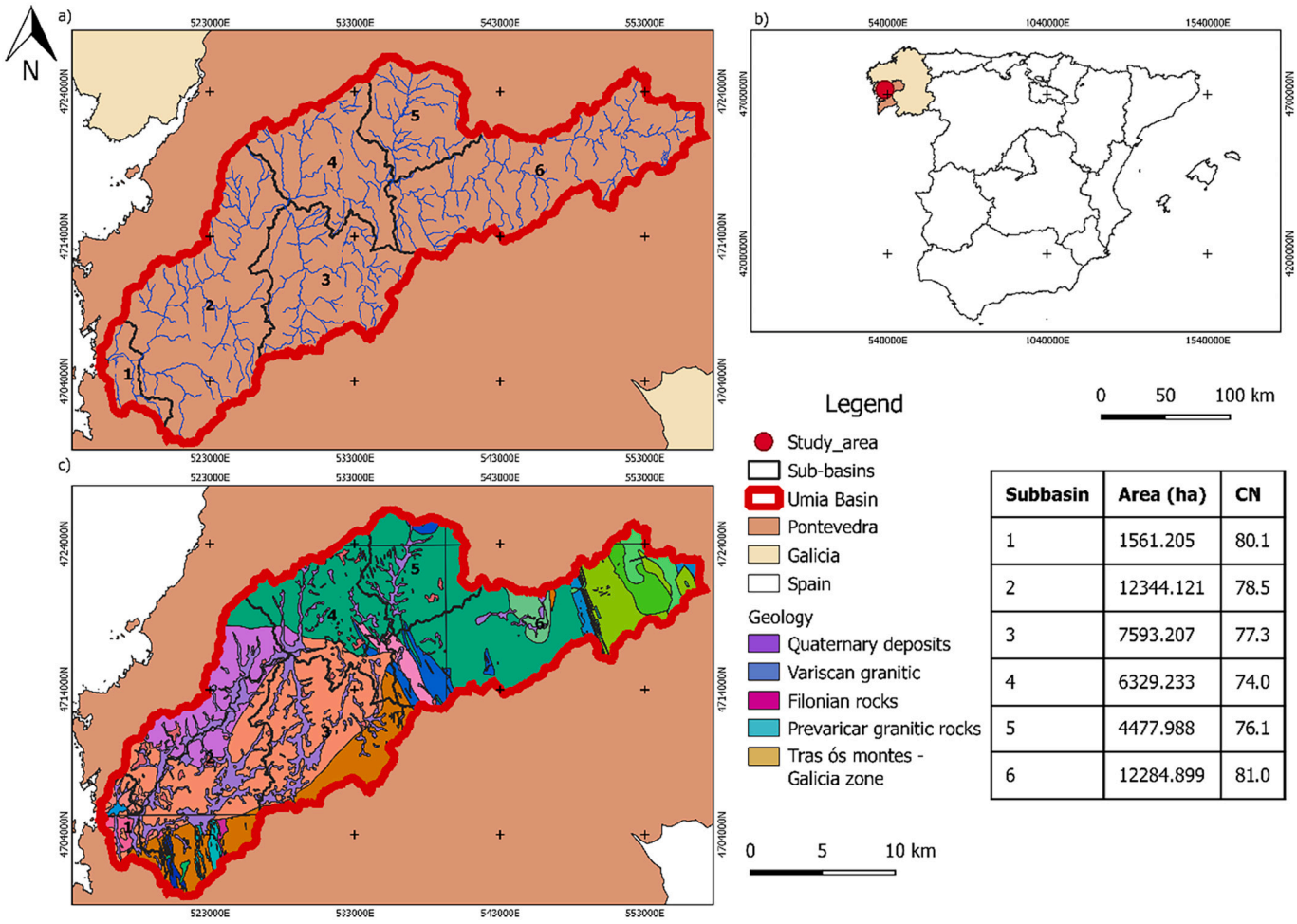

Subbasin	Area (ha)	CN
1	1561.205	80.1
2	12344.121	78.5
3	7593.207	77.3
4	6329.233	74.0
5	4477.988	76.1
6	12284.899	81.0

Fig. 1. (a) Location of Umia Basin and the subbasins in Pontevedra province; (b) location of study area on the Spain map. (c) Geology map of Umia Basin. The map coordinate system is EPSG:25829 ETRS89/UTM zone 29 N.

(SIOSE) (Gobierno de España, 2016) indicates that the basin's current distribution is 35% broad-leaved forest, 24.8% complex cultivation patterns, 15.6% moors and heathland, 10% coniferous forest and 15% other land uses. Major problems in the study area also include land abandonment, whose impact on the forestry sector increases the risk of forest fires, and issues such as the selection of fast-growing forest species and high population dispersion. In the agricultural sector, on the other hand, the size of farms is limited due to the characteristic smallholdings of this territory, leading to intensification of land use. This has also led to serious environmental problems such as the elimination of riparian vegetation, increases in pollutants in water as well as an increase in the risk of flooding. The study area characteristically floods each winter, when the rivers that make up the basin tend to overflow at least once, and there are major economic and social impacts due to the flooding of agricultural land, commercial premises and homes, damage to infrastructure and occasional accidents (Xunta de Galicia, 2015).

Augas de Galicia, the devolved regional body in charge of flood risk analysis, has analysed the risk of flooding in the area over time, highlighting serious flooding that has led to the cutting of roads and the isolation of populated areas. Other historical events recorded that highlight the high risk of flooding in the area are the collapse of a bridge in the municipality of Bayón (in 1875), a death in the municipality of Portas (1978) and flooding of multiple homes and businesses (2009, 2010, 2011) (Xunta de Galicia: Augas de Galicia, 2021). Between 2005 and 2017, records show 1010 accidents caused by floods in the municipality of Vilagarcía de Arousa and 199 in the municipality of Caldas de Reis. The total financial losses in the area due to flooding have not been estimated, but Augas de Galicia is in the process of implementing a project proposing measures worth €232,607, plus projects detailing the flooding of the area to the tune of €945,000. All this highlights the need to obtain answers and information on flood risks in the study area, to assess the qualities of the area and the real potential for reducing the risk of flooding on the river.

2.2. Land use classification

2.2.1. Satellite images

The data used in this study are from Sentinel-2 images taken in 2015, 2016 and 2021. There are two Sentinel-2 satellites: Sentinel-2A launched in 2015 and Sentinel-2B in 2017. Both have a 10-day revisit cycle (Drusch et al., 2012). The multispectral imagery (MSI) onboard took images at 13 different spectral bands, with a spatial resolution varying from 10 m to 60 m. These images are all freely downloadable from the ESA website (Copernicus Open Access Hub, 2021). They provide very good spectral information and are suitable for land cover dynamics (Grinand et al., 2013). The images were collected on the same or similar dates, so those for the different years show the same land surface areas.

Images were downloaded from the Copernicus Open Access Hub repository at Level 1C (L1C) with the top of atmosphere (TOA) values and Level 2A (L2A) already corrected to bottom of the atmosphere (BOA) values with Sen2Cor. The image from 2016 is a sentinel Level-1 Product and the one from 2021 year is Level 2A. Not all Sentinel-2 images are atmospherically corrected so TOA reflectance of Sentinel-2

Table 1
The available Sentinel-2 images for this study.

Season	Image data	Sensor	Precision
Summer	08/08/2016	S2A_MSI_L1C	77.86
	17/08/2021	S2B_MSI_2A	83.18
Autumn	15/11/2015	S2A_MSI_L1C	66.94
	18/11/2021	S2B_MSI_2A	59.48
Winter	14/03/2016	S2A_MSI_L1C	78.18
	15/03/2021	S2A_MSI_2A	65.42
Spring	20/05/2016	S2A_MSI_L1C	53.38
	19/05/2021	S2B_MSI_2A	84.96

images from Level 1C were used in this study. The Level-1C Sentinel-2 images were converted to the physical measure of TOA correction using the Dark Object Subtraction (DOS) method (Chavez, 1988), which is an image-based technique. DOS methods assume that non-zero signal values over supposedly zero-value dark shaded pixels are atmospheric scattering signals. The DOS1 method used in this study is available in the Semi-Automatic Classification Plug-in (SCP) version within QGIS software (Moran et al., 1992). The method is fully automatic and requires no additional input settings. One of the main objectives of this methodology is to obtain a cloud-free classification due to the influence of cloud cover and summer rainfall. This paper uses a cloud cover percentage of <2%. In addition, the bands used in the classification were resampled to 10 m pixel size with the corresponding calibration and atmospheric correction, the 20 m bands of the imagery were resampled to 10 m in order to harmonize all band data and ensure that the classification of images was adjusted to this resolution.

2.2.2. Image classification

One image from every season was selected, and the image classification and precision were determined (Table 1). In cases where a given month had multiple images the criterion of cloud cover percentage was selected. The highest precision obtained is for summer season images, as shown in the results. The images selected for classification were collected on 8th august 2016 and on 17th august 2021. This same methodology was used with an image from 25th July 2015 (necessary for the calibration and validation of the flood model), but hardly any differences were found with the 2016 image.

Performing area change dynamics is a multi-step process (Holland et al., 2006), in which all steps add value to the accuracy of the results. Broadly, the methodology proposed consists of three major stages: pre-processing; image classification and accuracy assessment.

Pre-processing focuses mainly on the consideration of spectral, radiometric and spatial aspects of the images, as these treatments contribute greatly to the quality of the expected results (Butt et al., 2015). First, the spectral bands were combined for each date to form multi-spectral images. Second, a radiometric correction of the images was carried out, as this was pre-processing to improve the spectral value of a satellite image taken by a sensor. Atmospheric corrections for remote sensing data were mainly made based on image statistics, empirical methods, tools and the radiative transfer model. The pre-processed multi-spectral Sentinel images were input into the SCP in QGIS for classification.

Next, training areas are set up. Accurate training plot data are essential for supervised classification. The basis for delineating training area polygons was the most representative coverage of land cover, and the classes were set via photointerpretation via a combination of Sentinel-2 images with different colour compositions. Orthophoto images available from the National Aerial Orthophoto Programme (PNOA) (Ministerio de Transporte Movilidad y Agenda Urbana, 2021). obtained during a photogrammetric flight in 2017, were used for photointerpretation. The PNOA images were used for training and verification, and field trips for validation were made in 2021. In addition, Google Street View was used to supplement the reference data. The polygons for each class were distributed homogeneously, avoiding statistical dependence, resulting in a total of 263 polygons encompassing a total of 44,556 pixels, corresponding to 0.73% of the basin. Four macro classes were set up and ten classes (Table 2) were selected to depict the land cover and land changes in the Umia Basin. They were distributed across all six sub-basins (division for subsequent hydrological analysis).

Table 2
Descriptions of land use and land cover types defined in the study area.

Macro classes	Classes	Code	Description
Rural	Agriculture	1	Agriculture land typically land devoted to agriculture.
	Bare ground	2	Land with vegetative cover loss.
	Vineyard	9	Land with plantation of grapevines used in winemaking.
	Garden	4	A piece of ground adjoining a house, in which grass, flowers, and shrubs may be grown.
Forest	Riparian vegetation	5	Vegetation along the riverbanks, which has been influenced by the dynamic water table.
	Scrub	7	Area of land covered with short trees and bushes (h < 4 m)
	Trees	8	Area of land covered with trees (h > 4 m)
Anthropogenic	Road	6	A wide way paved
	Buildings	3	Structures with a roof and walls, houses, and factories.
Water	Water	10	Rivers, reservoirs, and wetlands.

Images were then classified out via Random Forest (RF). This is a specific machine learning technique based on the iterative, random creation of decision trees. First, the input features and classes were defined. RF calculates several random decision trees based on (1) the number of training samples and (2) the number of trees. The more trees there are, the more accurate the model is, but the longer the calculation time is. RF creates several decision trees randomly using the Gini coefficient to split them. A model based on the decision trees is thus created and used to classify all the pixels. A pixel is classified according to the majority vote of the decision trees. The number of training samples was 5000 and the number of trees was 500.

The next step was accuracy assessment, which is necessary to assess the reliability of the results. The Error of Commission (EC), Error of Omission (EO), Producer Accuracy (PA) and User Accuracy (UA) were computed based on an error matrix resulting from accuracy assessment. EO is linked to the classified results and is supplemented by PA. They refer to items that are left out of their correct class in the classification. EC represents classified values that were predicted to be in a particular class but do not belong to that class. It is supplemented by UA. In this study an advance accuracy assessment using the SCP (Semi-Automatic Classification Plug-in) functions for the RF classifier was performed. Using the land cover classification map generated, the next analytical step was to run a post-processing tool to obtain the reports from each classifier, which provide the pixel sum and area coverage of each land cover class. Accuracy assessment requires these parameters to calculate the total number of training samples required for the image classified using Eq. 1.

$$N = \left(\sum_{i=1}^{c} \frac{(W_i S_i)}{S_0} \right)^2 \quad (1)$$

where $W_i$is the area of the mapped portion of class i, S_i is the standard deviation of stratum i, S_0 is the expected standard deviation of overall accuracy and c is the total number of classes.

Finally, post-classification or change detection were carried out. Change detection is relevant in image analysis because it enables gains or losses in the land classes identified to be determined (Valdivieso-Ros et al., 2021). To determine the extent and trends of land cover changes in the Umia basin, post-classification change detection was employed. This involved the use of images from 2016 and 2021 to check for changes in the interim period. The surface areas of changes, including the transition matrix and class statics, were calculated.

2.3. Model simulations

This study runs and analyses different simulations based on a hydrological model of the Umia River Basin. Those simulations are calculated from a hydrological model obtained with HEC-HMS software (V.4.9.0), calibrated and validated with data from 2014 to 2016 which enables inputs (i.e. hydrographs) to be obtained for the hydrological model of the simulations proposed. To obtain the hydrological model of the study area, a digital terrain model was obtained from the National Centre for Geographic Information, specifically from the National Aerial Orthophotography Programme (PNOA) (National Geographic Institute of Spain, 2021)(Spanish National Geographic Institute, 2021). The land uses taken for calibration and validation were obtained from Sentinel-2 data according to the methodology described above. Precipitation and evaporation data were obtained from Meteogalicia (Xunta de Galicia, 2021), from a total of 6 atmospheric stations (Appendix A.1), with the weighted average precipitation of each station being calculated using the Thiessen polygon method. Flow data were obtained from the website of the Ministry for Ecological Transition (2020) from two monitoring stations in the study area, one downstream and one upstream (Appendix A.2). The hydrological model was calibrated by comparing the simulated and previously observed values for each of the eight biggest rainfall events in 2014 and 2015 (Appendix A.3). The model was calibrated using two different methods, but on the same dates, to check which one gave better results. The two methods used were the Soil Conservation Service (SCS) Curve Number Method and the Clark Method. Other parameters were calculated: The time of concentration was added to the data for the corresponding sub-basin (hours), while the lag time was added to the data for each corresponding reach (minutes). Finally, a check was performed on the robustness of the model drawn up to confirm that the results obtained were reasonable and consistent with expectations (Razi et al., 2010)(Razi et al., 2010). The sampling strategy chosen required 6 HEC-HMS model runs for each type of calibration and 6 for validation. This enabled us to economise on analysis time while still obtaining optimal calibration and validation results. Some authors suggest that calibration across the entire available dataset may be preferable for parameter identification (S. K. Singh and Bárdossy, 2012), but most published work still advocates the split-sample strategy (Arsenault et al., 2018; Gaborit et al., 2015), hence the event-driven approach. The HEC-HMS model was calibrated and validated using the calibration and validation strategy of calibrating the model parameters per sub-basin from upstream to downstream, as per Zhang et al. (2022). The confirmation check was performed on the four biggest rainfall events of 2016 (Appendix A.3.).The calibration process using the SCS curve number method gives a result of $R^2 = 0.96$, while the Clark method gives $R^2 = 0.98$. Both these figures are very high. In the validation check for the SCS curve number method $R^2 = 0.95$, while in that for the Clark Method $R^2 = 0.99$. The "coefficient of performance of error series A" (CPA) and CPA' were calculated for model validation (Table A.4.). Different studies suggested this common method for the assessment of time series agreement by examining the sum of squared differences (Babel et al., 2004; Najim et al., 2006). The results indicate that the HEC-HMS model is well optimised in this study and that the HEC-HMS model is generally reliable and robust for flood simulation in this study area.

For the simulations the infiltration capacity was quantified in a parameter derived by the Soil Conservation Service (SCS) called CN. This parameter determines the runoff over an area based on soil type, soil cover and the hydrological group of the soil (Cronshey, 1986). The figure calculated for sub-basin 1 is 80.1, for sub-basin 2 it is 78.5, for sub-basin 3 it is 77.3, for sub-basin 4 it is 74.0, for sub-basin 5 it is 76.1 and for sub-basin 6 it is 81.0. To better assess the possible effects of using NBS, four hypothetical scenarios were chosen. These scenarios were based on changing the land use from agriculture to forestry. According to Perpiña Castillo et al. (2020), Galicia has one of with the highest percentages of abandoned agricultural land of any region in Spain, with an estimated figure of around 44%. Therefore, a change of 44% of the agricultural area to forestry was simulated, prioritising the less permeable soils. The hydrographs simulated in HEC-HMS were carried out for three events that caused flooding in the Umia Basin. Event 1 took place from 22/02/2021 to 26/02/2021, event 2 from 04/12/2021 to 11/12/2021 and event 3 from 02/01/2022 to 15/01/2022.

In addition, the scenarios designed envisage different situations. The first corresponds to current status (Observed), i.e. the current land use scenario, in which the hydrological models represent land use changes in 2021. The remaining scenarios reflect the decision to reduce flood hazard by implementing NBS and by afforestation. The afforestation of the head of the basin was therefore simulated in the upstream afforestation scenario (S-Up). In this scenario afforestation was designed for sub-basins 6 and 5, increasing their forest area from 3475.790 ha to 7342.49 ha and from 2235.10 ha to 3194.86 ha respectively. Next afforestation in the lower part of the basin was simulated in the downstream afforestation scenario (S-Down), where afforestation in the hydrological model in sub-basins 4 and 3 increased their areas by 904.59 ha and 1525.65 ha respectively. The last scenario (S-Total) assessed afforestation throughout the basin, analysing the optimal status in the whole basin. Specifically, the land use changes described in simulations S-Up and S-Down were used, plus changes in sub-basins 2 and 1, where forest area was increased by 44.09% and 75.28% respectively. In addition to these simulations, events were calculated with land uses from the 2016 classification (S-2016). The Flow Chart of the methodology described here can be seen in Fig. 2, and a table summarising information sources can be found in Appendix A.5.

2.4. Environmental, economic and social analysis

To assess the environmental, social and economic costs and benefits of each simulation in the basin, an analysis was carried out to assess the cost of afforestation and the benefits that the use of these NBS could bring. These simulations were carried out via cost-benefit analysis (CBA), which seeks to analyse the extent to which project benefits (values of use and non-use) exceed costs (in this case, the cost of investment and maintenance). The main assessment criterion is thus economic efficiency. First, all costs and benefits must be selected and expressed in monetary values. This monetisation is critical for analysis, particularly when environmental effects are studied. Secondly, the net present value (NPV) of the project must be calculated. The NPVs of the different afforestation scenarios here were calculated by using a discount rate of 4% and a series of future costs (negative values) and ecosystem service benefits (positive values). Assuming "n" is the number of cash flows in the list of values (eq. 2):

$$NPV = \sum_{i=1}^{n} \frac{values_i}{(1 + rate)^i} \quad (2)$$

Where, "values$_i^{"}$ is the net cash inflow-outflows during a single period and "i, "is the discount rate or return that could be earned in alternative investments.

To assess the overall environmental benefits provided by the use of these NBS, this analysis relies on previous studies (e.g. Dittrich et al., 2019; Johnen et al., 2020) which seek to assess ecosystem services (ES). Due to the limitations of the study reported here, whose main objective is not to assess environmental benefits but rather how land use and NBS affect flood risk, ES are assessed using benefit transfers. Thus, the results of existing studies are transferred in order to determine the monetary value for the present area. It is necessary to obtain similar background conditions; in this case the study focuses on using study values from temperate European forests.

2.4.1. Environmental and social benefits

Dittrich et al. (2019) and Johnen et al. (2020) use an estimated value of €281.05/ha/year to assess biodiversity. In this way, the biodiversity

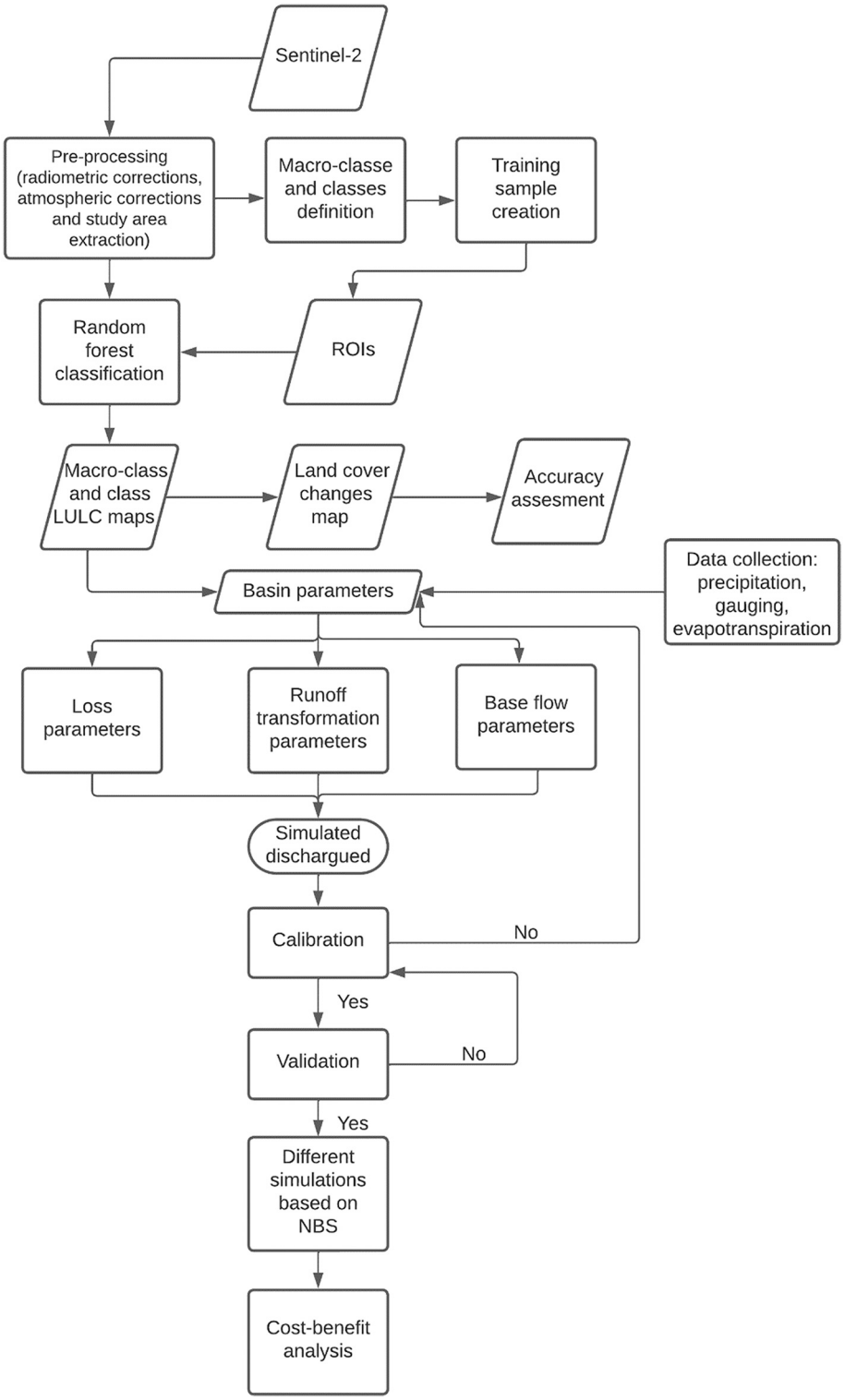

Fig. 2. Flow diagram followed in the methodology in the Umia River Basin.

services of use and non-use are quantified, and double counting is avoided. This includes use values and "non-use values such as existence value (the benefit people get from the mere knowledge that wildlife exists even if they never see it) and bequest value (the benefit people get from knowing that wildlife will be protected and conserved for the benefit of future generations)". The impact of the afforestation area has also been assessed via carbon sequestration, based on the database developed by Bernal et al. (2018) for different types of forest restoration actions worldwide and the consequent carbon sequestration rates (IUCN, 2018). The afforestation area for each scenario was multiplied by the relevant carbon price of €15.41/tCO_2 (OECD, 2016), and by the carbon sequestration rates per hectare in tonnes (based on the removal rate database for Spain and Galicia with the restoration type "Pine"), which was 7.7 CO_2/ha/year. This corresponds to the average value from the time of reforestation up to 20 years of tree life. The CO_2 uptake value increases as trees grow during and decreases when the stand stabilises.

The use of NBS, and in particular afforestation, could have a positive effect on surface and groundwater quality (Duffy et al., 2020). Broadmeadow and Nisbet (2004) explain this on the grounds that by obtaining a more balanced hydrological regime, from the reduction of maximum and minimum flows, the extent of flooding is reduced and groundwater recharge is controlled to a greater extent. This would reduce the amount of nutrients and sediment that reach the river, reservoir or aquifer. There is also the filtering capacity provided by reforestation in the riparian areas from which they originate, which reduces the risk of flooding. Müller et al. (2019) conduct a systematic review that quantifies these benefits of reforestation in relation to surface and groundwater quality. In their study they find a wide range from USD25 to 2227/ha/year, with most values being between USD25/ha/year and USD211/ha/year. The low values for providing clean drinking water may be influenced by the generally large amount of clean water available, which results in a low willingness to pay. However, water quality is a growing issue because it is assumed that this number will tend to rise. Therefore, in this estimation the highest value is selected and converted to euros, resulting in a figure of €187/ha.

2.4.2. Cost of NBS implementation

Afforestation costs were calculated based on the expanded forest area in each simulation. To that end, agricultural land was converted to forest land use. First, the price of the area to be afforested must be determined. Seeking to curtail the abandonment of rural land in Galicia, the administration permits abandoned land to become part of the "Banco de Tierras" (Land Bank) (Ley 11/2021, 2021). These plots can be rented, thus facilitating their use for measures to mitigate climate change, fight fires or, in this case, mitigate the risk of flooding. The Xunta de Galicia (the public administration with authority over land management in Galicia) makes the land available to the public at a price. In this case study, the rental price per hectare is €105/ha/year (Agader, 2020). This figure was multiplied by 20 (years) for the surface area reforested in each sub-basin. The costs of deforestation also need to be quantified. These were obtained from the average figures based on the regulations set by the administration. A value of €2526.45/ha was obtained for actions covering land preparation. It is estimated that 3 mechanised pruning operations are required at a cost of €474.76/ha each.

The benefits include improvements in water quality, CO_2 sequestration capacity, the value of biodiversity (both use and non-use) and recreational value. All necessary costs are factored in, from obtaining the plots, preliminary actions, soil preparation, the price of plants and other forestry actions. The analysis was drawn up for 20 years, due to the type of plantation selected.

3. Results and discussion

3.1. classification of land use

The Umia Basin was classed under four macro-classes that included the ten classes considered here for a period of 5 years (2016 and 2021), as shown in Fig. 3. Given the hydrological characteristics of the basin, the biggest area in 2016 (Fig. 3a) was Riparian Vegetation, which covered 10,886.53 ha (24.43% of the entire basin). The rivers of the Galicia-Costa Hydrological Demarcation, to which the Umia River belongs, extend over more than 14,700 km (Augas de Galicia, 2015) and their drainage network has a highly branched dendritic distribution, typical of the terrain. The surface of the Umia River basin thus comprises one main channel and several tributaries, which in turn have several tributaries of their own. As a result a large percentage of the area is occupied by riparian vegetation associated with these rivers and streams. The smallest area is that occupied by water, which comprises 0.91% of the basin. In 2021 (Fig. 3b) there was a slight improvement in some classes. The areas that occupy most land were tree zones, which covered 10,911 ha (24.49% of the basin), while riparian vegetation covered 9721.68 ha (21.82%). As in 2016, the area that occupied least territory was Water, but the coverage was 0.15% greater in 2021. The first case may be due to differences between hydrological years, i.e. 2016 was a drier year and with less depth of water in the water bodies than in 2021 (Xunta de Galicia, 2021), when more water was available.

An analysis of the sub-basins shows similar results for 2016 (Fig. 2c) and 2021 (Fig. 3d): 53% of the surface area of sub-basin 1 is given over to the Rural macro-class, 44.58% of sub-basin 2 was Forest in 2016 and 48.87% in 2021, while 45.66% was classed as Rural in 2016 and 41.48% in 2021. These are the areas closest to the coast, so their land covers are typically mosaics of housing, agriculture, gardens, etc.. In sub-basins 3, 4, 5 and 6 the most representative land cover classes are Forest, which accounts for around 60%, with an increase of between 4 and 8% from 2016 to 2021. Forest uses, especially those associated with afforestation, become more characteristic of this territory as we move away from the coast. Galicia has just over 2 million hectares of forest, of which 70% is woodland and 30% scattered trees (Dirección General de Medio Natural y Política Forestal, 2011). The management systems of these forests are currently based on the logging of conifers (39.15%) and hardwoods (60.85%), especially *Pinus pinaster* (47.64%) and *Pinus radiata* (44.86%) in the first case and *Eucalyptus spp.* (95.2%) for hardwoods (Ministerio para la Transición Ecológica y el Reto Demográfico, 2020).

Once the classifications by classes and their distribution have been analysed, a common approach for accuracy assessment involves computing an error matrix from independent ground survey observations or from visual interpretation of high-resolution images to quantify class-specific accuracies and overall map accuracy. According to the 2016 error matrix classified under the RF method (Table 3), the class that covered most land based in the pixel count was Trees (10,244 pixels). By contrast Garden use covered the least land in pixel counts with a total of 997. The overall precision obtained was 77.86%. with Riparian Vegetation and Scrub being the classes most often misclassified, with an EC value of 0.73. The error matrices for the 2021 classification (Tables 4 and 4.1) show an overall precision of 83.18%, with Riparian Vegetation as the most misclassified class, with an EC value of 0.79. Water was the most successfully classified class in both years, with the lowest EO value, followed by Garden. The accuracy of the method depends on several factors such as the number of training samples, the number of land cover classes, the type of terrain and the pre-processing techniques applied to images (Phiri et al., 2020). Taking into account the complexity of comparing results in terms of accuracy with similar research using RF as a classifier, a pixel-based classification method and four classes in general, the accuracy level obtained ranges between 65 and 95% (Denize et al., 2018; Fragoso-Campón et al., 2018; Immitzer et al., 2016; Khaliq et al., 2018; Steinhausen et al., 2018; Vuolo et al., 2018), which is similar to that of 77–83% found in the present research. The main difference is the greater number of classes used, i.e. 10. (See Table 3.1.)

Comparing 2016 and 2021, the area covered by Agriculture increased, with the Vineyard class accounting for 24.81% (1492.87 ha) of the total (Table 5). After field checks, it has been proven that this is due to recently established vineyards. Therefore, with no foliage, with the posts installed and the land ploughed, the classification method used assumes that this is agricultural land. This contrasts with the financial grants from the regional government (Xunta de Galicia). For example, it is estimated that the vineyard area in Rías Baixas (the Designated Origin for vineyards in this area) increased by 50 ha in 2019 and 130 ha in 2021 (Xunta de Galicia, 2022). Therefore, in recent years vine growing has been intensifying and areas that were abandoned are being recovered. Vineyard, Riparian Vegetation and Agriculture classes misclassed as Bare Ground account for 21.78% (762.4 ha), 18.66% (653.33 ha) and 17.77% (622.03 ha) respectively of the total. In the first case, this may be due to the absence of foliage and to ploughed soil for new plantations. In the second case it may be due to the replacement of this vegetation by vineyards. And in the case of agriculture, there may be changes in seasonal crops that show a different spectral image.

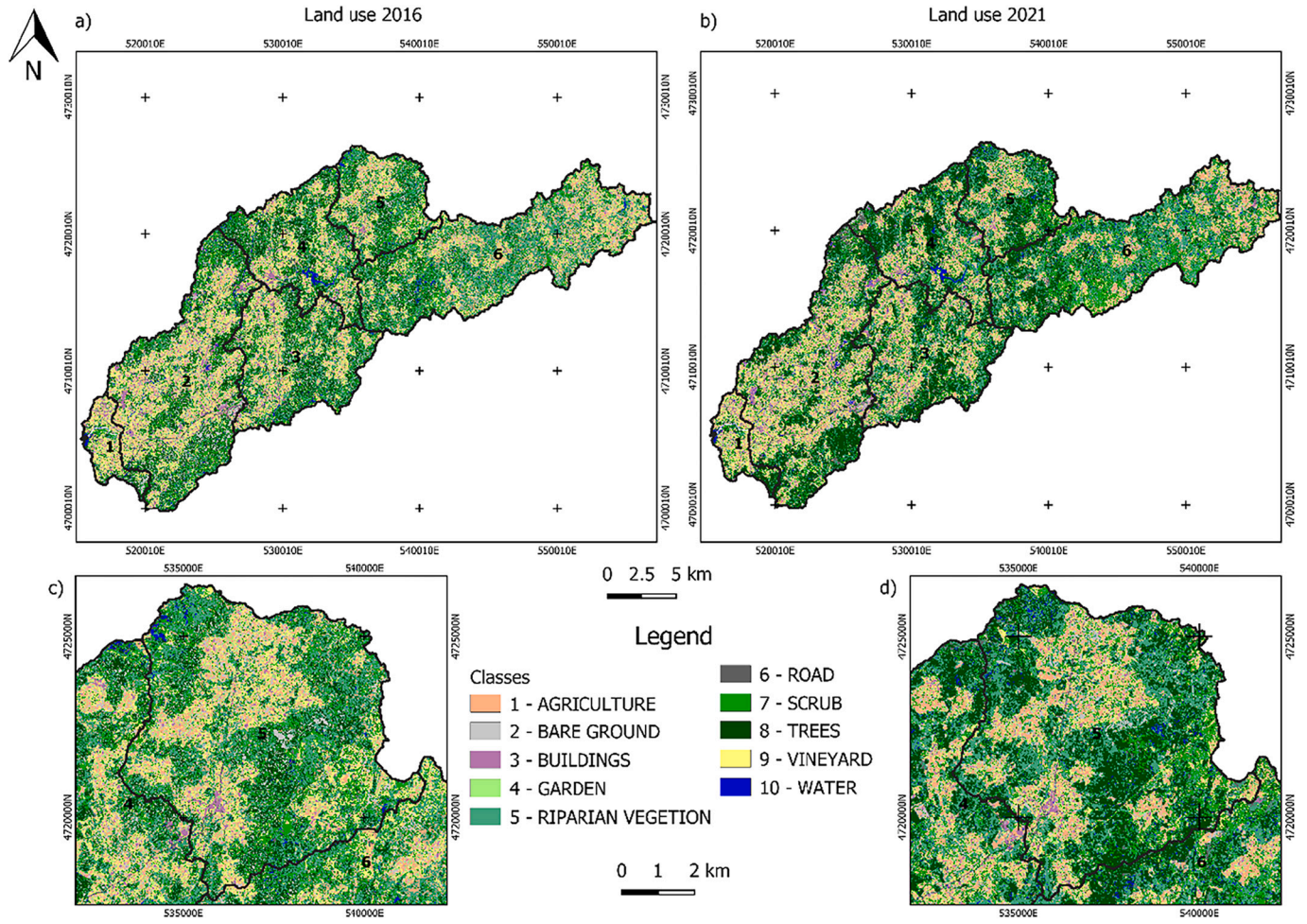

Fig. 3. Land use classification maps of Umia Basin (a) 2016-year; (b) 2021 year; (c) Detail of subbasin 5, 2016-year; (d) Detail of subbasin 5, 2021 year.

Table 3
Error matrix land use pixel count 2016 year.

	Reference										
Classified	1	2	3	4	5	6	7	8	9	10	Total
1	**978**	192	16	33	27	13	3	131	412	1	1806
2	122	**1095**	97	5	21	1	56	1601	182	0	3180
3	23	56	**3419**	2	0	158	16	0	2	8	3684
4	140	28	21	**307**	1	27	3	8	264	0	799
5	258	6	1	1	**708**	35	27	1497	98	64	2695
6	0	0	70	5	4	**1640**	7	3	1	53	1783
7	70	38	0	3	58	1	**802**	1824	212	17	3025
8	138	72	0	0	86	15	182	**4877**	26	27	5423
9	137	127	5	12	36	8	10	156	**2324**	6	2821
10	0	0	20	0	56	166	26	147	1	**7067**	7483
Total	1866	1614	3649	368	997	2064	1132	10,244	3522	7243	**32,699**

Acquiring large-scale training data to train the RF classifier in the classification of complex regions with a great many categories is a laborious task that requires hours of processing. Thus, in the present study we assumed that training samples should represent approximately 0.25% of the total study area used by the RF classifier for large-scale classification (Colditz, 2015; Deng and Wu, 2013; Du et al., 2015). Once these errors in classification have been identified, it is useful to carry out work with more training areas that include this category of "new vineyard", since its spectral signature after 5 years of growth is totally different from what it looks like in the year of planting. Considering the study area and the strong influence of the wine sector in it, this is an issue that can be improved in future studies.

In satellite image analysis, the number of images used differs widely, from two images per season (Carrasco et al., 2019) or two images per month (Malinowski et al., 2020) to 150 images per season (Nguyen et al., 2020) or two images per land cover classification (Mohamed and El-Raey, 2019). The literature reviewed concludes that with 2–5 images per year the success rate exceeds 70%. In addition, large-scale image processing requires long computation times and high storage capacity. In this study, two images per year were selected, including the seasons in which the greatest variations take place in the vegetation, and specifically cloud-free (<2%).

Finally, the type of land ownership in the study area must be highlighted: it is characterised by smallholdings. According to the land register (Ministerio de Hacienda y Función Publica, 2022), the

Table 3.1
Area based error matrix land use classification 2016 year.

	Reference												
Classified	1	2	3	4	5	6	7	8	9	10	Area	Wi	EC
1	**0.0276**	0.0054	0.0005	0.0009	0.0008	0.0004	0.0001	0.0037	0.0116	0	57,244,800	0.051	0.4588
2	0.0014	**0.0126**	0.0011	0.0001	0.0002	0	0.0006	0.0184	0.0021	0	41,132,100	0.0366	0.6548
3	0.0001	0.0002	**0.0117**	0	0	0.0005	0.0001	0	0	0	14,128,000	0.0126	0.0714
4	0.0031	0.0006	0.0005	**0.0067**	0	0.0006	0.0001	0.0002	0.0058	0	19,714,600	0.0176	0.6193
5	0.0093	0.0002	0	0	**0.0255**	0.0013	0.001	0.0538	0.0035	0.0023	108,865,300	0.0969	0.7368
6	0	0	0.0003	0	0	**0.0076**	0	0	0	0.0002	9,260,400	0.0082	0.0617
7	0.0013	0.0007	0	0.0001	0.0011	0	**0.0147**	0.0334	0.0039	0.0003	62,143,800	0.0553	0.7351
8	0.0015	0.0008	0	0	0.0009	0.0002	0.002	**0.0537**	0.0003	0.0003	67,008,200	0.0597	0.1005
9	0.0027	0.0025	0.0001	0.0002	0.0007	0.0002	0.0002	0.0031	**0.0455**	0.0001	62,013,300	0.0552	0.1772
10	0	0	0.0016	0	0.0045	0.0135	0.0021	0.0119	0.0001	**0.5731**	681,531,100	0.6069	0.0555
Total	0.0469	0.023	0.0158	0.0081	0.0338	0.0242	0.0208	0.1782	0.0728	0.5765	**1,123,041,600**		
Area	52,697,103	25,859,352	17,727,116	9,085,078	37,918,623	27,129,228	23,394,333	200,095,854	81,754,254	647,380,658	**1,123,041,600**		
SE	0.0009	0.0006	0.0004	0.0004	0.0011	0.0011	0.0007	0.0015	0.0008	0.0016			
SE area	1,017,032	636,409	468,084	396,831	1,182,490	1,201,827	744,001	1,730,289	950,667	1,837,929			
95% CI area	1,993,382	1,247,362	917,444	777,788	2,317,681	2,355,580	1,458,243	3,391,366	1,863,308	3,602,340			
PA [%]	58.8261	54.7709	73.9643	83.3779	75.4243	31.3968	70.4265	30.1164	62.4896	99.4226			
UA [%]	54.1528	34.434	92.8067	38.423	26.2709	91.9798	26.5124	89.9318	82.3821	94.4407			
EO	0.4127	0.4521	0.2594	0.1625	0.2433	0.6872	0.2966	0.6986	0.3750	0.0055	0		

Total precision [%] = 77.8632.
The area is represented in m2, SE is the standard error, CI the confidence interval, PA the produce's accuracy and UA the user's accuracy.

Table 4
Error matrix land use pixel count 2021 year.

	Reference										
Classified	1	2	3	4	5	6	7	8	9	10	Total
1	**1142**	52	27	32	17	6	99	132	483	0	1990
2	71	**1418**	93	13	14	10	80	51	97	0	1847
3	7	48	**3188**	5	0	115	1	0	2	6	3372
4	60	19	16	**296**	1	12	20	23	120	0	567
5	75	6	1	3	**712**	9	12	1916	42	60	2836
6	10	0	49	5	5	**1851**	0	2	0	2	1924
7	291	26	6	5	59	2	**821**	206	189	0	1605
8	19	7	0	0	135	11	21	**7810**	18	19	8040
9	191	35	6	9	14	5	78	54	**2571**	0	2963
10	0	3	263	0	40	43	0	50	0	**7156**	7555
Total	1866	1614	3649	368	997	2064	1132	10,244	3522	7243	**32,699**

Table 4.1
Area based error matrix land use classification 2021 year.

	Reference												
Classified	1	2	3	4	5	6	7	8	9	10	Area	Wi	EC
1	**0.0307**	0.0014	0.0007	0.0009	0.0005	0.0002	0.0027	0.0036	0.013	0	60,176,600	0.0536	0.4283
2	0.0012	**0.0239**	0.0016	0.0002	0.0002	0.0002	0.0014	0.0009	0.0016	0	35,003,400	0.0312	0.2339
3	0	0.0002	**0.0105**	0	0	0.0004	0	0	0	0	12,524,300	0.0112	0.0540
4	0.0018	0.0006	0.0005	**0.0087**	0	0.0004	0.0006	0.0007	0.0035	0	18,617,800	0.0166	0.4821
5	0.0023	0.0002	0	0.0001	**0.0217**	0.0003	0.0004	0.0585	0.0013	0.0018	97,216,800	0.0866	0.7994
6	0.0001	0	0.0003	0	0	**0.0102**	0	0	0	0	11,848,500	0.0106	0.0377
7	0.0092	0.0008	0.0002	0.0002	0.0019	0.0001	**0.026**	0.0065	0.006	0	57,101,700	0.0508	0.4891
8	0.0002	0.0001	0	0	0.0016	0.0001	0.0003	**0.0944**	0.0002	0.0002	109,110,000	0.0972	0.0278
9	0.0023	0.0004	0.0001	0.0001	0.0002	0.0001	0.0009	0.0006	**0.0303**	0	39,268,900	0.035	0.1343
10	0	0.0002	0.0211	0	0.0032	0.0035	0	0.004	0	**0.5754**	682,173,600	0.6074	0.052
Total	0.0478	0.0278	0.035	0.0101	0.0294	0.0152	0.0322	0.1691	0.056	0.5774	**1,123,041,600**		
Area	53,649,953	31,208,250	39,321,635	11,382,744	32,978,510	17,068,932	36,109,372	189,953,309	62,873,507	648,495,387	**1,123,041,600**		
SE	0.0009	0.0005	0.0013	0.0004	0.0009	0.0006	0.0007	0.0011	0.0008	0.0016			
SE area	975,005	506,385	1,468,603	444,881	1,035,291	624,932	820,732	1,252,205	890,377	1,776,053			
95% CI area	1,911,009	992,515	2,878,461	871,966	2,029,170	1,224,867	1,608,635	2,454,321	1,745,138	3,481,064			
PA [%]	64.3682	86.1093	30.1129	85.3867	74.0089	66.7818	80.8904	55.7972	54.194	99.6377			
UA [%]	57.3869	76.7731	94.5433	52.2046	25.1058	96.2058	51.1526	97.1393	86.7702	94.7187			
EO	0.3577	0.1402	0.7000	0.1470	0.2593	0.3419	0.1950	0.4421	0.4579	0.0034			

Total precision [%] = 83.1840.
The area is represented in m2, SE is the standard error, CI the confidence interval, PA the produce's accuracy and UA the user's accuracy.

Table 5
Conversion matrix of land changes in the Umia basin from 2016 to 2021 (ha).

	1	2	3	4	5	6	7	8	9	10	Total
1	**1549.56**	622.03	123.53	451.91	984.62	63.26	804.22	272.05	830.89	22.41	5724.48
2	724.86	**400.42**	103.43	202.56	486.99	14.52	543.51	1226.45	394.06	16.41	4113.21
3	246.98	141.82	**643.62**	109.08	32.43	89.67	31.31	16.24	77.02	24.63	1412.8
4	699.57	210.1	80.39	**259.32**	53.31	41.53	194.43	37.02	394.44	1.35	1971.46
5	445.38	653.33	41.4	108.94	**4415.67**	197.25	1493	3004.37	363.43	163.72	10,886.53
6	78.94	94.05	82.53	39.84	71.99	**424.28**	24.16	54.71	49	6.54	926.04
7	529.14	380.41	32.51	124.23	1593.86	116.73	**949.93**	2053.21	380.95	53.41	6214.38
8	239.58	216.63	19.15	58.64	1497.15	108.89	539.76	**3810.17**	144.14	66.71	6700.82
9	1492.87	762.4	119.72	504.34	522.23	74.6	1105.1	323.38	**1285.5**	11.16	6201.33
10	10.78	19.15	6.15	2.92	63.43	54.12	24.69	113.4	7.45	**103.83**	405.92
Total	6017.66	3500.34	1252.4	1861.8	9721.68	1184.85	5710.2	10,911	3926.9	470.17	**44,556.97**

perimeters of the plots add up to more than 1.3 million kilometres. Plots registered as rural land in Galicia have an average area of just 0.26 ha, and that figure drops to 0.17 ha in the study area. Galicia is also characterised by a widely dispersed population living in rural areas. This makes for mosaics that combine houses, farms, agricultural warehouses and small plots that range from seasonal crops of vegetables to fruit plantations, vineyards and forest. Classifying land uses under these conditions was a real challenge, and one that makes the results obtained even more significant.

3.2. Simulations

The hydrographs simulated in HEC-HMS were drawn up for three events that caused flooding in the Umia Basin (Fig. 4). Event 1 reached a

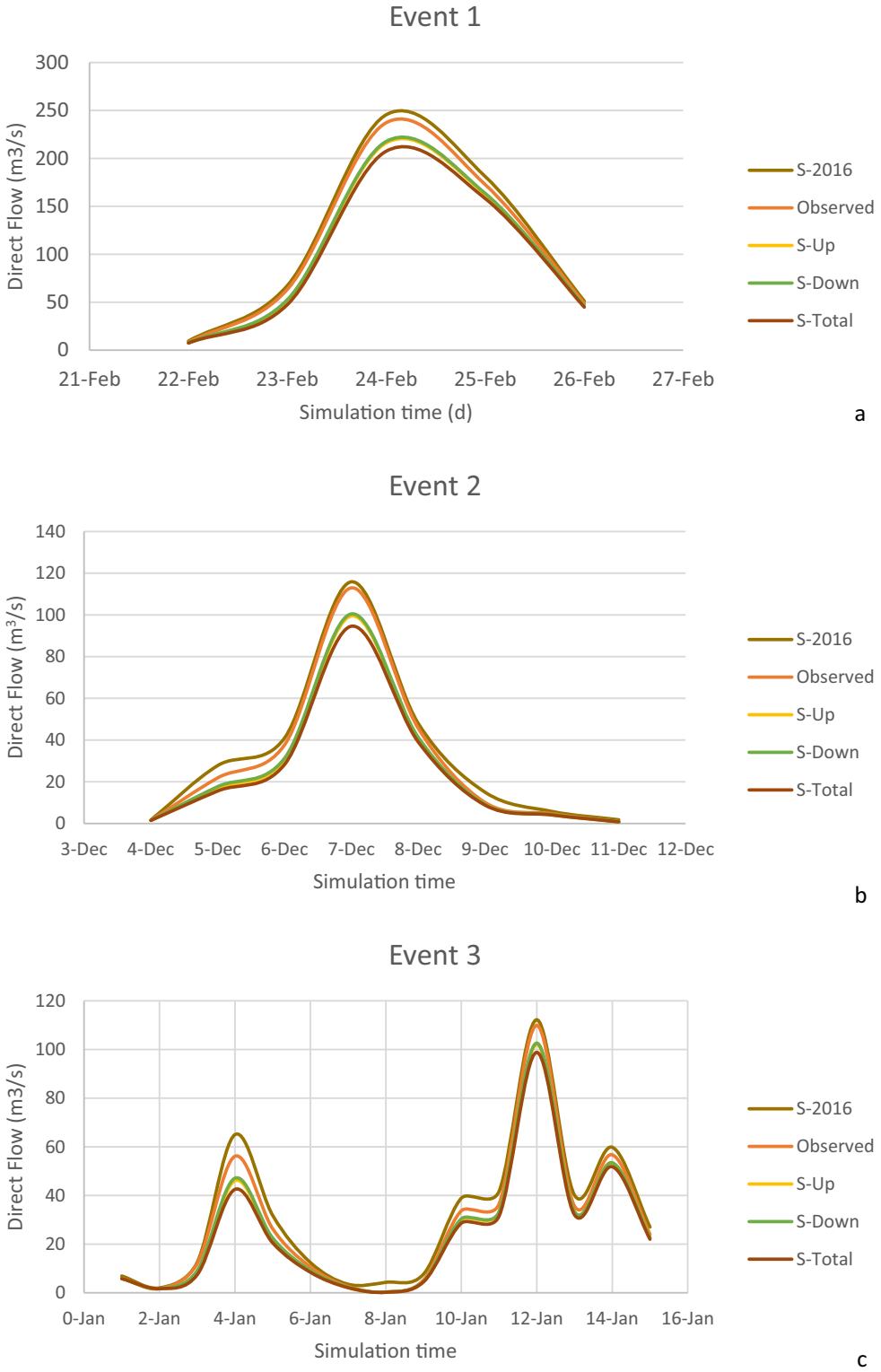

Fig. 4. Hydrographs obtained for three events from the model output considering the different scenarios, S-2016 (Events in the year 2021 simulated with 2016 land uses), "Observed" ("Current land use-Observed"), S-Up ("Forestation upstream"), and S-Down ("Forestation downstream") and S-Total ("Forestation everywhere").

flow rate of 237.3 m^3/s with the LULC resulting from the classification. However, this maximum flow was reduced for simulations S-Up (216.3 m^3/s), S-Down (217.8 m^3/s) and S-Total (207.6 m^3/s). This was also the case for events 2 and 3, where the maximum flow rates observed for these classifications were 113.00 (Event 2) and 109.9 (Event 3). The maximum flow rate for event 2 is that of S-Down (100.5m^3/s), followed by S-Up (99.5m^3/s), with S-Total (94.6) having the lowest figure. This coincides with the results for event 3, where S-Down gave a figure of 102.6m^3/s, followed by Observed (102.1m^3/s) and S-Down (98.8m^3/s). In all events the S-2016 simulation gives a higher peak flow rate than the actual observed value for the current land use in 2021. This may be due to the increase in forest area as discussed above. Statistical significance was analysed in comparisons of observed and simulated models, and from one simulated model to another. For all cases in each event the statistical significance is $p > 0.05$, so the null hypothesis is rejected. On the other hand, peak flow rate (m^3/s) was reduced by 8.9% (S-Up), 8.2% (S-Down) and 12.6% (S-Total) for the first event. Event 2 showed the greatest improvement, with reductions in peak flow rate of 11.9% (S-Up), 11.1% (S-Down) and 16.3% (S-Total), compared to reductions of 7.1% (S-Up), 6.6% (S-Down) and 10.1% (S-Total) for the third event. Apart from the substantial reduction in flow rate, a delay in it is also observed.

In event 1 (the event with the highest precipitation) the peak flow rate was delayed from 25 February at 12:00 to 24 February at 23:00, for example, but such delays were observed in all the simulations studied. This is very important for events of this type, especially in critical areas such as the reservoir in the study area, where this information could help manage the regulation of the reservoir outlet flow based on the expected flow and the expected time period. In fact, in the simulations where the upstream basins (S-Up and S-Total) were reforested, the maximum flow rate into the reservoir was reduced by 6.5%. Therefore, it could have a positive influence on the management of this infrastructure to reduce risks downstream or be proactive and ensure there is storage capacity for the expected flow. This reduction coincides with the statement in (Paleo, 2010) that the A Baxe reservoir is a paradigmatic example: it was designed by the administration to laminate the frequent floods in Caldas de Reis and also to produce electricity in addition to supplying drinking water to the communities in the area. However, this reservoir has shown little ability to laminate floods downstream, reducing but not eliminating the risk and causing the proliferation of *Microcystis* (Viso-Vázquez et al., 2021), which has caused a serious health problem due to the presence of toxins in the water (Acuña-Alonso et al., 2020). This is why the reservoir is under debate: not only has it not fulfilled the purpose for which it was built, but it also generates major problems for the population. This is in line with the study by Schoener (2022), where ponds are found have a minimal impact on transmission losses, highlighting that the impact is greatest in the lower part of the stream and decreases upstream.

The delay in the hydrographic basins thanks to the different land covers that intercept, capture and infiltrate rainwater and thus reduce surface runoff benefits society in terms of reducing the flood hazard (Brody et al., 2014) and increasing groundwater availability and reserves. In addition, it brings environmental benefits by reducing surface erosion and slowing the decrease in soil quality (Keesstra et al., 2018). However such afforestation has a limited effect (Danáčová et al., 2020), as also contrasted by Ellis et al. (2021). Experts also emphasise its important buffering effect, in contrast to the highly intensive agricultural and livestock use in the area (Álvarez et al., 2017). The effects of reforestation used as NBS also depend on the forest species used, given their differences in uptake (Zabret and Šraj, 2015). 76% of the study area falls into soil hydrological group type C (slow infiltration, 36–13 mm/h), 10% into type D (very slow infiltration, <13 mm/h) and only 14% into type A (fast infiltration >76 mm/h), which also influences the effective capacity of the NBS selected. This adds to the difficulty of solving the serious flooding problem in the Umia River Basin.

The greatest improvement is that found for simulation S-Total "Reforestation everywhere", where increasing the forest area in the whole catchment obviously modifies the roughness coefficient and reduces the flow there. The next best result is simulation S-Up, where reforestation was carried out upstream. This result is supported by other studies, where it is highlighted that improving water retention areas and upstream land use adaptations can be useful in reducing the frequency of floods in small catchments (Hooijer et al., 2004). Simulation S-Down, gives the poorest results, perhaps due to the importance of the upstream reduction, or to other parameters such as soil permeability or land use and the fact that the anthropogenic area (13.74% in sub-basin 3 and 12.86% in sub-basin 4) is larger than in upstream sub-basins 6 (8.83%) and 5 (9.83%). It may also be due to a combination of all these factors. This shows that for effective flood hazard management, actions must be designed for the areas where they have the most effects, i.e. headwaters or areas far from the river mouth in order to intercept as much water as possible and delay run-off. For flood regulation, there is a spatial link between downstream and upstream. The results of the simulations when NBS is applied upstream or downstream match those of Johnen et al. (2020), but it should be noted the different characteristics and layout of the type of plots in our study area, with highly heterogeneous land uses and very small plot sizes, means that comparison with other studies gives not highly significant findings. In the study by Klingner (2014), for example, 77% of the catchment is converted from cropland to forestry use with very good results, but such a high land use change seems unrealistic. As for where NBS should be applied, the headwaters and upstream areas comprising the supply zones are considered the best flood regulation area for a catchment (Syrbe and Walz, 2012). Actions at the river mouth do not significantly reduce hazards, though containment measures should focus there once an event occurs. Discharge capacity should also be increased (Vanneuville et al., 2016). This poses a challenge for the management of the territory (Hartmann et al., 2019), since reducing the risk of flooding impacts owners who do not suffer the consequences of that flooding. In addition, catchments with more diverse characteristics, including topography, soils and land use, such as the one studied here, are considered produce more complex results than more homogenous catchments (Knebl et al., 2005). The improved land cover data from the classification carried out, which will also enable information to be continually updated, improves on the information provided by other sources such as the Spanish Land Cover Information System (SIOSE), which takes a long time to update.

The nature of floods and the increasing need to study them in relation to climate change and land use change means that our study has numerous applications in research, operations and policy. The result of this study is a complete hydrological model for the Umia River Basin plus a comprehensive land use classification adapted to the characteristics of the study area. The model can be used for other relevant flooding issues in the region, and the methodology can be replicated in other areas. Other issues that could be included in future models include real-time rainfall and further simulations such as changes of use from anthropogenic to forestry. The study reported here has been adapted to land cover in the form of abandoned agricultural land, and thus provides a pragmatic model, as opposed to studies where all agricultural land is converted to forestry (Johnen et al., 2020). Another possibility would be simulations that consider increases and improvements in the riparian vegetation of the study area, given that the retention and filtering capacity of such vegetation is broadly proven. Food security is also of increasing concern: it could lead to a need to change land use from forestry to agriculture, thereby increasing NC (Singh et al., 2022). These simulations together with permeability maps can provide valuable information for decision-making and land-use planning. This information could indicate where land-use changes would be most appropriate. Other changes, such as increases in built-up areas, would increase surface runoff and thus lead to a small increase in peak discharge (Kabeja et al., 2020) which would be hard to modify once implemented. This highlights the importance of knowing permeability levels, land uses and regulatory status in order to optimise the development of environmental

governance in the study area. The methodology proposed here is key to achieving these purposes, combining the use of GIS tools (in a critical study area) and hydrological models accessible to the administration. An additional parameter that could affect the efficiency of these models, as highlighted by Knebl et al. (2005), is the use of CN. The use of CN in this study is derived from physical measurements, but it is an empirical parameter and could therefore be a limitation in these models. Other approaches, such as that of Green and Ampt (1911), whose use a physical methodological approach, could improve these models.

3.3. General discussion: economic and social repercussions

The possible environmental, economic and social impacts of the various scenarios were analysed and discussed. Environmental benefits such as biodiversity enhancement, water quality improvement and CO_2 sequestration, social benefits such as recreation and the cost of the NBS in each simulation were assessed. The total costs depend directly on the number of hectares, so the S-Down scenario is the one with the lowest total cost at €15,476,487.05, followed by the S-Up scenario at €29,580,643.24 and finally the S-Total, in which the whole basin is assumed to be reforested, at €65,158,130.15. Consequently, the NPVs obtained were €14.647.785,94 for S-Up, €7.663.669,36 for S-Down and €32.265.097,66 for S-Total. All three scenarios show a positive NPV for the period studied, so they are all economically sustainable. Johnen et al. (2020) find negative values in scenarios where the area to be reforested is larger. This is due to the high cost of land acquisition. In our case the regulations allow for the lease of abandoned land for the purpose of implementing measures to prioritise resilience to climate change. In addition, it is interesting to note the economic benefits of implementing any of these scenarios in terms of water quality in the basin. This is especially so for NBS in the upstream sub-basins (5 and 6), as there is a reservoir in sub-basin 4 with serious eutrophication problems caused by high levels of pollutants derived from land use (Acuña-Alonso et al., 2022).

The CBA thus shows that the benefits obtained from the simulations studied based on the use of NBS outweigh the costs. The areas of land classed as reforested in the simulations are the least permeable and most erosion-vulnerable soils. Cupać et al. (2020) highlight that measures on such land bring more financial benefit than cost, which would encourage their financing. Taking all these implications into account, the most favourable scenarios would be S-Up and S-Total. Furthermore, considering the flow-rates studied in the events that caused flooding (Fig. 3) in the study area, these are also the scenarios with the greatest hazard reduction. It is also interesting to note the value of the investment required, which is much higher in S-Total than in S-Up, as it involves the whole basin. Flood hazard management must focus on reducing flood risk but also on improving environmental, societal and economic benefits (Vanneuville et al., 2016). Le Coent et al. (2021) analyse three studies comparing the use of NBS and grey structures, and find that in all cases the cost is lower for the use of NBS. In fact, for the same level of damage avoided, NBS solutions are between 15% and 63% less expensive than grey solutions. Furthermore, for the cost of infrastructure to be positive it must incorporate all the direct and indirect benefits brought to the ecosystem, not just the reduction in flow-rate. In a context of limited public resources, financial valuation can help to identify the right solution for addressing water risks, and the analysis of NBS, grey or even hybrid structures can help identify the most appropriate strategy for each case (Raška et al., 2022).

There is a need for coordinated management policies. For example, the results of this study where part of the riverside vegetation is replaced by agriculture, mostly vineyards, stand out. This is covered by current regulations, under which prior authorisation to cultivate is not required in areas subject to easement (5 m from the river bank) but it is necessary to forest these areas (Ministerio de Obras Públicas y Urbanismo, 1986). Attention is also focused on the Forestry Act of Galicia (Act 7/2012, 2012), under which changes from forestry to agriculture are allowed under certain conditions to increase the viability of agricultural holdings. Thus, farming interests and detriment to forestry are linked. However the opposite situation holds if a change from agricultural use to forestry is desired: only rural land classed as being for agricultural use but in a state of abandonment and assigned to a farming land bank (minimum 2 years) is permitted, and then only with prior notification of the forestry management body and when 1) it is adjacent to forest lands; and 2) enclaves of up to 5 ha of woodland are formed. In both cases lush deciduous trees must be used. The latter case has recently been modified by the Act on the Recovery of Farm Land in Galicia (Act 11/2021, 2021), but was in force until May 2021. Therefore, the regional forestry, farming and water public domain regulations have not helped to reduce flood risks, because they encourage changes from forestry to farmland and hinder the afforestation of the territory, especially riparian areas. This highlights the need for multidisciplinary legislation with a comprehensive approach.

Finally, it should be noted that the challenge in reducing flood risk and hazard lies in a comprehensive management of the territory, with land uses planned according to the host capacity of each area. It is important for proper planning to include simulations of future scenarios to improve decision-making by managers and enabling them to anticipate potential future risks, especially in climate change scenarios. In this case, information from satellite images, geographic information systems and flood risk simulation make up a combination that provides a useful tool for decision making, starting with better, more detailed, more precise, current data.

4. Conclusions

Land cover change in the Umia Basin, made up of very small, heterogeneous plots averaging just 0.47 ha each, was successfully mapped with Sentinel-2 images with an OA of 77% and 83%. This is the first case study on this type of characteristic smallholdings. The basin underwent noticeable changes in land use over the 5-year period. The use classes of Agriculture, Road, Trees and Water all increased on 2016. By contrast, 26.15% of land classed as Riparian Vegetation changed to scrub during the study period. Future research needs to consider including "New Vineyards" as a new training class, as the absence of foliage in recently established vineyards resulted in their being misclassified as agricultural land. Stand-out features include the large number of plots and different species, changes in cutting, ages and vegetation on the same plots. This methodology is thus considered as useful for this type of plots (0.26 ha on average). This classification was useful to simulate the flood hazard in the study area. These two tools are very useful but had not been combined until now. For the three precipitation events in 2016 that caused flooding in the study area, different NBS actions were simulated based on the reforestation of specific areas and were compared with the actual situation. The resulting hydrograph estimated peak discharges of 237.3 m^3/s (Event 1), 113.00 m^3/s (Event 2) and 109.9 m^3/s (Event 3). For the simulations carried out there is a reduction of 8.9% in the case of afforestation in headwater areas, 8.6% in actions throughout the basin and 13.0% for afforestation downstream. This percentage of reduction can be seen as a success given the low filtering capacity of the soil in the area, where 86% of the land is classed as slow or very slow filtering. Remote sensing from satellite images offers an opportunity to model responses to precipitation events. This makes for progress in and improvement of land management. All three scenarios show positive NPVs for the period studied, so they are all economically sustainable. There is a need for measures to increase water retention throughout the basin and to facilitate discharge at the mouth. These measures are reported to have social, economic and environmental benefits, which are quantified to value NBS as a sustainable tool that improves territorial planning. All this is done via a comprehensive approach supported by new, coordinated, multi-sectoral policies.

Data availability

Data will be made available on request.

Acknowledgements

This research was funded by the Universidade de Vigo (convocatoria de axudas propias á investigación da Universidade de Vigo para o ano 2021) under project 21VI-01. Financial support was also provided by mobility grants from the University of Vigo (C.A.A.). Funding for open access charges was from the Universidade de Vigo/CISUG. A.N. wishes to thank the Universidade de Vigo for the grant Axudas Predoutorais para a formación de Doutores 2019 (grant number 00VI 131H 6410211).

Appendix A. Supplementary data

Supplementary data to this article can be found online at https://doi.org/10.1016/j.ecoinf.2022.101777.

References

Acuña-Alonso, C., Álvarez, X., Lorenzo, O., Cancela, Á., Valero, E., Sánchez, Á., 2020. Water toxicity in reservoirs after freshwater algae harvest. J. Clean. Prod. 124560 https://doi.org/10.1016/j.jclepro.2020.124560.

Acuña-Alonso, C., Álvarez, X., Valero, E., Pacheco, F.A.L., 2022. Modelling of threats that affect Cyano-HABs in an eutrophicated reservoir: First phase towards water security and environmental governance in watersheds. Sci. Total Environ. 809, 152155.

Agader. Xunta de Galicia, 2020. Agader. Precios de referencia arrendamento. Https://Agader.Xunta.Gal/Sites/W_pagade/Files/Documentacion/Prezos_referencia_2020_pontevedra.Pdf.

Álvarez, X., Valero, E., Santos, R.M.B., Varandas, S.G.P., Sanches Fernandes, L.F., Pacheco, F.A.L., 2017. Anthropogenic nutrients and eutrophication in multiple land use watersheds: Best management practices and policies for the protection of water resources. Land Use Policy 69, 1–11. https://doi.org/10.1016/j.landusepol.2017.08.028.

Arasumani, M., Singh, A., Bunyan, M., Robin, V.V., 2021. Testing the efficacy of hyperspectral (AVIRIS-NG), multispectral (Sentinel-2) and radar (Sentinel-1) remote sensing images to detect native and invasive non-native trees. Biol. Invasions 1–17.

Arnold, J.G., Srinivasan, R., Muttiah, R.S., Williams, J.R., 1998. Large area hydrologic modeling and assessment part I: model development 1. JAWRA J. Am. Water Res. Associat. 34 (1), 73–89.

Arsenault, R., Brissette, F., Martel, J.-L., 2018. The hazards of split-sample validation in hydrological model calibration. J. Hydrol. 566, 346–362. https://doi.org/10.1016/j.jhydrol.2018.09.027.

Augas de Galicia, 2015. Plan Hidrolóxico Galicia-Costa 2015–2021.

Avand, M., Moradi, H.R., Ramazanzadeh Lasboyee, M., 2021. Spatial prediction of future flood risk: an approach to the effects of climate change. Geosciences 11 (1). https://doi.org/10.3390/geosciences11010025.

Bernal, B., Murray, L.T., Pearson, T.R.H., 2018. Global carbon dioxide removal rates from forest landscape restoration activities. Carbon Bal. Manag. 13 (1), 1–13.

Brillinger, M., Henze, J., Albert, C., Schwarze, R., 2021. Integrating nature-based solutions in flood risk management plans: A matter of individual beliefs? Sci. Total Environ. 795, 148896 https://doi.org/10.1016/j.scitotenv.2021.148896.

Broadmeadow, S., Nisbet, T.R., 2004. The effects of riparian forest management on the freshwater environment: a literature review of best management practice. Hydrol. Earth Syst. Sci. 8 (3), 286–305.

Brody, S., Blessing, R., Sebastian, A., Bedient, P., 2014. Examining the impact of land use/land cover characteristics on flood losses. J. Environ. Plan. Manag. 57 (8), 1252–1265.

Bruzzone, L., Bovolo, F., Paris, C., Solano-Correa, Y.T., Zanetti, M., Fernández-Prieto, D., 2017. Analysis of multitemporal Sentinel-2 images in the framework of the ESA Scientific Exploitation of Operational Missions. In: 2017 9th International Workshop on the Analysis of Multitemporal Remote Sensing Images (MultiTemp), pp. 1–4.

Butt, A., Shabbir, R., Ahmad, S.S., Aziz, N., 2015. Land use change mapping and analysis using Remote Sensing and GIS: A case study of Simly watershed, Islamabad, Pakistan. Egypt. J. Remote Sens. Space Sci. 18 (2), 251–259.

Carrasco, L., O'Neil, A.W., Morton, R.D., Rowland, C.S., 2019. Evaluating combinations of temporally aggregated Sentinel-1, Sentinel-2 and Landsat 8 for land cover mapping with Google Earth Engine. Remote Sens. 11 (3), 288.

Chavez, P.S., 1988. An improved dark-object subtraction technique for atmospheric scattering correction of multispectral data. Remote Sens. Environ. 24 (3), 459–479. https://doi.org/10.1016/0034-4257(88)90019-3.

Chowdhuri, I., Pal, S.C., Chakrabortty, R., 2020. Flood susceptibility mapping by ensemble evidential belief function and binomial logistic regression model on river basin of eastern India. Adv. Space Res. 65 (5), 1466–1489.

Colditz, R.R., 2015. An evaluation of different training sample allocation schemes for discrete and continuous land cover classification using decision tree-based algorithms. Remote Sens. 7 (8), 9655–9681.

Collentine, D., Futter, M.N., 2018. Realising the potential of natural water retention measures in catchment flood management: Trade-offs and matching interests. J. Flood Risk Manag. 11 (1), 76–84.

Copernicus Open Access Hub. (2021).

Cowles, A.G.H., 2021. Effects of Historical Land-use Change on Surface Runoff and Flooding in the Amite River Basin, Louisiana, USA Using Coupled 1D/2D HEC-RAS–HEC-HMS Hydrological Modeling.

Cronshey, R., 1986. Urban hydrology for small watersheds (Issue 55). US Department of Agriculture, Soil Conservation Service, Engineering Division.

Cupać, R., Trbić, G., Zahirović, E., 2020. Cost–benefit analysis of climate change adaptation measures in Bosnia and Herzegovina. Euro-Mediterranean J. Environ. Integrat. 5 (2), 26. https://doi.org/10.1007/s41207-020-00160-4.

Danáčová, M., Földes, G., Labat, M.M., Kohnová, S., Hlavčová, K., 2020. Estimating the effect of deforestation on runoff in small mountainous Basins in Slovakia. Water 12 (11), 3113.

Deng, C., Wu, C., 2013. The use of single-date MODIS imagery for estimating large-scale urban impervious surface fraction with spectral mixture analysis and machine learning techniques. ISPRS J. Photogramm. Remote Sens. 86, 100–110.

Denize, J., Hubert-Moy, L., Corgne, S., Betbeder, J., Pottier, E., 2018. Identification of winter land use in temperate agricultural landscapes based on Sentinel-1 and 2 Times-Series. In: IGARSS 2018–2018 IEEE International Geoscience and Remote Sensing Symposium, pp. 8271–8274.

Dewan, A.M., Yamaguchi, Y., 2009. Land use and land cover change in Greater Dhaka, Bangladesh: Using remote sensing to promote sustainable urbanization. Appl. Geogr. 29 (3), 390–401. https://doi.org/10.1016/j.apgeog.2008.12.005.

Dirección General de Medio Natural y Política Forestal, 2011. Cuarto inventario forestal nacional. Ministerio de Medio Ambiente y Medio Rural y Marino, Centro de Publicaciones.

Dittrich, R., Ball, T., Wreford, A., Moran, D., Spray, C.J., 2019. A cost-benefit analysis of afforestation as a climate change adaptation measure to reduce flood risk. J. Flood Risk Manag. 12 (4), e12482 https://doi.org/10.1111/jfr3.12482.

Drusch, M., Del Bello, U., Carlier, S., Colin, O., Fernandez, V., Gascon, F., Hoersch, B., Isola, C., Laberinti, P., Martimort, P., Meygret, A., Spoto, F., Sy, O., Marchese, F., Bargellini, P., 2012. Sentinel-2: ESA's optical high-resolution mission for GMES operational services. Remote Sens. Environ. 120, 25–36. https://doi.org/10.1016/j.rse.2011.11.026.

Du, P., Samat, A., Waske, B., Liu, S., Li, Z., 2015. Random forest and rotation forest for fully polarized SAR image classification using polarimetric and spatial features. ISPRS J. Photogramm. Remote Sens. 105, 38–53.

Duffy, C., O'Donoghue, C., Ryan, M., Kilcline, K., Upton, V., Spillane, C., 2020. The impact of forestry as a land use on water quality outcomes: an integrated analysis. Forest Policy Econ. 116, 102185.

Ellis, N., Anderson, K., Brazier, R., 2021. Mainstreaming natural flood management: A proposed research framework derived from a critical evaluation of current knowledge. Progr. Phys. Geogr. Earth and Environment 45 (6), 819–841.

Ford, D., Pingel, N., DeVries, J.J., 2002. Hydrologic Modeling System HEC-HMS: Applications Guide. US Army Corps of Engineers, Hydrologic Engineering Center.

Forkuor, G., Dimobe, K., Serme, I., Tondoh, J.E., 2018. Landsat-8 vs. Sentinel-2: examining the added value of sentinel-2's red-edge bands to land-use and land-cover mapping in Burkina Faso. GIScience & Remote Sens. 55 (3), 331–354.

Fragoso-Campón, L., Quirós, E., Mora, J., Gutiérrez, J.A., Durán-Barroso, P., 2018. Accuracy enhancement for land cover classification using LiDAR and multitemporal sentinel 2 images in a forested watershed. In: Proceedings, Vol. 2. https://doi.org/10.3390/proceedings2201280. Issue 20.

Gaborit, É., Ricard, S., Lachance-Cloutier, S., Anctil, F., Turcotte, R., 2015. Comparing global and local calibration schemes from a differential split-sample test perspective. Can. J. Earth Sci. 52 (11), 990–999.

Gobierno de España, 2016. SIOSE. Sistema de Información de Ocupación del Suelo de España. Ministerio de Transportes, Movilidad y Agencia Urbana. https://www.siose.es/.

Green, W.H., Ampt, G.A., 1911. Studies on soil phyics. J. Agric. Sci. 4 (1), 1–24.

Grinand, C., Rakotomalala, F., Gond, V., Vaudry, R., Bernoux, M., Vieilledent, G., 2013. Estimating deforestation in tropical humid and dry forests in Madagascar from 2000 to 2010 using multi-date Landsat satellite images and the random forests classifier. Remote Sens. Environ. 139, 68–80. https://doi.org/10.1016/j.rse.2013.07.008.

Halwatura, D., Najim, M.M.M., 2013. Application of the HEC-HMS model for runoff simulation in a tropical catchment. Environ. Model. Softw. 46, 155–162.

Hartmann, T., Slavíková, L., McCarthy, S., 2019. Nature-based solutions in flood risk management. In: Nature-based flood risk management on private land. Springer, Cham, pp. 3–8.

Holland, D.A., Boyd, D.S., Marshall, P., 2006. Updating topographic mapping in Great Britain using imagery from high-resolution satellite sensors. ISPRS J. Photogramm. Remote Sens. 60 (3), 212–223. https://doi.org/10.1016/j.isprsjprs.2006.02.002.

Hooijer, A., Klijn, F., Pedroli, G.B.M., Van Os, A.G., 2004. Towards sustainable flood risk management in the Rhine and Meuse river basins: synopsis of the findings of IRMA-SPONGE. River Res. Appl. 20 (3), 343–357. https://doi.org/10.1002/rra.781.

Immitzer, M., Vuolo, F., Atzberger, C., 2016. First experience with sentinel-2 data for crop and tree species classifications in Central Europe. Remote Sens. 8 (3) https://doi.org/10.3390/rs8030166.

IUCN, 2018. Global Emissions and Removals Databases. Https://Infoflr.Org/What-Flr/Global-Emissions-and-Removals-Databases.

Johnen, G., Sapač, K., Rusjan, S., Zupanc, V., Vidmar, A., Bezak, N., 2020. Modelling and Evaluation of the Effect of Afforestation on the Runoff Generation Within the Glinščica River Catchment (Central Slovenia).

Kabeja, C., Li, R., Guo, J., Rwatangabo, D.E.R., Manyifika, M., Gao, Z., Wang, Y., Zhang, Y., 2020. The impact of reforestation induced land Cover change

(1990–2017) on flood peak discharge using HEC-HMS hydrological model and satellite observations: a study in two mountain basins, China. Water 12 (5). https://doi.org/10.3390/w12051347.
Kalantari, Z., Lyon, S.W., Jansson, P.-E., Stolte, J., French, H.K., Folkeson, L., Sassner, M., 2015. Modeller subjectivity and calibration impacts on hydrological model applications: An event-based comparison for a road-adjacent catchment in south-east Norway. Sci. Total Environ. 502, 315–329. https://doi.org/10.1016/j.scitotenv.2014.09.030.
Keesstra, S., Nunes, J., Novara, A., Finger, D., Avelar, D., Kalantari, Z., Cerdà, A., 2018. The superior effect of nature based solutions in land management for enhancing ecosystem services. Sci. Total Environ. 610, 997–1009.
Khaliq, A., Peroni, L., Chiaberge, M., 2018. Land cover and crop classification using multitemporal sentinel-2 images based on crops phenological cycle. In: 2018 IEEE Workshop on Environmental, Energy, and Structural Monitoring Systems (EESMS), pp. 1–5.
Klingner, W., 2014. The Effects of Increased Infiltration and Distributed Storage on Reducing Peak Discharges in an Agricultural Iowa Watershed: the Middle Raccoon River. The University of Iowa.
Knebl, M.R., Yang, Z.-L., Hutchison, K., Maidment, D.R., 2005. Regional scale flood modeling using NEXRAD rainfall, GIS, and HEC-HMS/RAS: a case study for the San Antonio River Basin Summer 2002 storm event. J. Environ. Manag. 75 (4), 325–336. https://doi.org/10.1016/j.jenvman.2004.11.024.
Le Coent, P., Graveline, N., Altamirano, M.A., Arfaoui, N., Benitez-Avila, C., Biffin, T., Calatrava, J., Dartee, K., Douai, A., Gnonlonfin, A., Hérivaux, C., Marchal, R., Moncoulon, D., Piton, G., 2021. Is-it worth investing in NBS aiming at reducing water risks? Insights from the economic assessment of three European case studies. Nature-Based Solut. 1, 100002 https://doi.org/10.1016/j.nbsj.2021.100002.
Leavesley, G.H., Restrepo, P.J., Markstrom, S.L., Dixon, M., Stannard, L.G., 1996. The modular modeling system (MMS): User's manual. In: US Geological Survey Open-File Report, 96 (151,142).
Ley 11/2021, 2021. de 14 de mayo, de recuperación de la tierra agraria de Galicia.
Ley 7/2012, 2012. de 28 de junio, de montes de Galicia.
Malinowski, R., Lewiński, S., Rybicki, M., Gromny, E., Jenerowicz, M., Krupiński, M., Nowakowski, A., Wojtkowski, C., Krupiński, M., Krätzschmar, E., 2020. Automated production of a land cover/use map of Europe based on Sentinel-2 imagery. Remote Sens. 12 (21), 3523.
Mattos, T.S., Oliveira, P.T.S., de Bruno, L.S., Carvalho, G.A., Pereira, R.B., Crivellaro, L. L., Lucas, M.C., Roy, T., 2022. Towards reducing flood risk disasters in a tropical urban basin by the development of flood alert web application. Environ. Model. Softw. 151, 105367 https://doi.org/10.1016/j.envsoft.2022.105367.
McGrane, S.J., 2016. Impacts of urbanisation on hydrological and water quality dynamics, and urban water management: a review. Hydrol. Sci. J. 61 (13), 2295–2311.
Ministerio de hacienda y función publica, 2022. Catastro. Https://Www.Catastro.Meh.Es/.
Ministerio de Obras Públicas y Urbanismo, 1986. Real Decreto 849/1986, de 11 de abril, por el que se aprueba el Reglamento del Dominio Público Hidráulico, que desarrolla los títulos preliminar I, IV, V, VI y VII de la Ley 29/1985, de 2 de agosto, de Aguas. https://www.boe.es/buscar/act.php?id=BOE-A-1986-10.
Ministerio de Transporte Movilidad y Agenda Urbana, 2021. Plan Nacionall de Ortofotografía Aérea (PNOA).
Ministerio para la Transición Ecológica y el Reto Demográfico, 2020. Anuario de Estadística Forestal. Gobierno de España. https://www.mapa.gob.es/es/desarrollo-rural/estadisticas/aef_2018_documentocompleto_tcm30-543070.pdf.
Mohamed, S.A., El-Raey, M.E., 2019. Land cover classification and change detection analysis of Qaroun and Wadi El-Rayyan lakes using multi-temporal remotely sensed imagery. Environ. Monit. Assess. 191 (4), 1–19.
Moran, M.S., Jackson, R.D., Slater, P.N., Teillet, P.M., 1992. Evaluation of simplified procedures for retrieval of land surface reflectance factors from satellite sensor output. Remote Sens. Environ. 41 (2), 169–184. https://doi.org/10.1016/0034-4257(92)90076-V.
Müller, A., Knoke, T., Olschewski, R., 2019. Can existing estimates for ecosystem service values inform forest management? Forests 10 (2), 132.
Nakamura, R., Shimatani, Y., 2021. Extreme-flood control operation of dams in Japan. J. Hydrol. Reg. Stud. 35, 100821 https://doi.org/10.1016/j.ejrh.2021.100821.
Nath, B., Ni-Meister, W., Choudhury, R., 2021. Impact of urbanization on land use and land cover change in Guwahati city, India and its implication on declining groundwater level. Groundw. Sustain. Dev. 12, 100500.
Nguyen, H.T.T., Doan, T.M., Tomppo, E., McRoberts, R.E., 2020. Land Use/land cover mapping using multitemporal Sentinel-2 imagery and four classification methods—A case study from Dak Nong, Vietnam. Remote Sens. 12 (9), 1367.
Novo, A., Fariñas-Álvarez, N., Martínez-Sánchez, J., González-Jorge, H., Fernández-Alonso, J.M., Lorenzo, H., 2020. Mapping forest fire risk—a case study in Galicia (Spain). Remote Sens. 12 (22) https://doi.org/10.3390/rs12223705.
Paleo, U.F., 2010. Las dimensiones de las inundaciones históricas en Galicia en la comunicación del riesgo. Riesgos Naturales En Galicia 39.
Perpiña Castillo, C., Coll Aliaga, E., Lavalle, C., Martínez Llario, J.C., 2020. An assessment and spatial modelling of agricultural land abandonment in Spain (2015–2030). Sustainability Vol. 12 (2). https://doi.org/10.3390/su12020560.
Phiri, D., Simwanda, M., Salekin, S., Nyirenda, V.R., Murayama, Y., Ranagalage, M., 2020. Sentinel-2 data for land cover/use mapping: a review. Remote Sens. 12 (14), 2291.
Qiu, C., Mou, L., Schmitt, M., Zhu, X.X., 2019. Local climate zone-based urban land cover classification from multi-seasonal Sentinel-2 images with a recurrent residual network. ISPRS J. Photogramm. Remote Sens. 154, 151–162.
Rajkhowa, S., Sarma, J., 2021. Climate change and flood risk, global climate change. In: Global Climate Change. Elsevier, pp. 321–339.
Raška, P., Bezak, N., Ferreira, C.S.S., Kalantari, Z., Banasik, K., Bertola, M., Bourke, M., Cerdà, A., Davids, P., Madruga de Brito, M., Evans, R., Finger, D.C., Halbac-Cotoara-Zamfir, R., Housh, M., Hysa, A., Jakubínský, J., Solomun, M.K., Kaufmann, M., Keesstra, S., Hartmann, T., 2022. Identifying barriers for nature-based solutions in flood risk management: An interdisciplinary overview using expert community approach. J. Environ. Manag. 310, 114725 https://doi.org/10.1016/j.jenvman.2022.114725.
Razi, M.A.M., Ariffin, J., Tahir, W., Arish, N.A.M., 2010. Flood estimation studies using hydrologic modeling system (HEC-HMS) for Johor River, Malaysia. J. Appl. Sci. 10 (11), 930–939.
Refshaard, J.C., Storm, B., 1995. MIKE SHE. Computer Models of Watershed Hydrology, pp. 809–846.
Sánchez-Espinosa, A., Schröder, C., 2019. Land use and land cover mapping in wetlands one step closer to the ground: Sentinel-2 versus landsat 8. J. Environ. Manag. 247, 484–498.
Schoener, G., 2022. Impact of urbanization and stormwater infrastructure on ephemeral channel transmission loss in a semiarid watershed. J. Hydrol. Reg. Stud. 41, 101089 https://doi.org/10.1016/j.ejrh.2022.101089.
Seddon, N., Chausson, A., Berry, P., Girardin, C.A.J., Smith, A., Turner, B., 2020. Understanding the value and limits of nature-based solutions to climate change and other global challenges. Philos. Trans. R. Soc. B 375 (1794), 20190120.
Sekertekin, A., Marangoz, A.M., Akcin, H., 2017. Pixel-based classification analysis of land use land cover using Sentinel-2 and Landsat-8 data. Int. Arch. Photogramm. Remote. Sens. Spat. Inf. Sci. 42, 91–93.
Singh, S.K., Bárdossy, A., 2012. Calibration of hydrological models on hydrologically unusual events. Adv. Water Resour. 38, 81–91.
Singh, V., Lohani, A.K., Jain, S.K., 2022. Reconstruction of extreme flood events by performing integrated real-time and probabilistic flood modeling in the Periyar river basin, Southern India. Nat. Hazards 112 (3), 2433–2463. https://doi.org/10.1007/s11069-022-05272-4.
Spanish National Geographic Institute, 2021. Spanish National Plan for Orthophotography (PNOA).
Steinhausen, M.J., Wagner, P.D., Narasimhan, B., Waske, B., 2018. Combining Sentinel-1 and Sentinel-2 data for improved land use and land cover mapping of monsoon regions. Int. J. Appl. Earth Obs. Geoinf. 73, 595–604.
Syrbe, R.-U., Walz, U., 2012. Spatial indicators for the assessment of ecosystem services: providing, benefiting and connecting areas and landscape metrics. Ecol. Indic. 21, 80–88.
Thanh Noi, P., Kappas, M., 2018. Comparison of random forest, k-nearest neighbor, and support vector machine classifiers for land cover classification Using Sentinel-2 imagery. Sensors 18 (1). https://doi.org/10.3390/s18010018.
Valdivieso-Ros, C., Alonso-Sarria, F., Gomariz-Castillo, F., 2021. Effect of different atmospheric correction algorithms on sentinel-2 imagery classification accuracy in a semiarid mediterranean area. Remote Sens. 13 (9), 1770.
Vanneuville, W., Wolters, H., Scholz, M., Werner, B., Uhel, R., 2016. Flood Risks and Environmental Vulnerability: Exploring the Synergies between Floodplain Restoration, Water Policies and Thematic Policies.
Viso-Vázquez, M., Acuña-Alonso, C., Rodríguez, J.L., Álvarez, X., 2021. Remote detection of cyanobacterial blooms and chlorophyll-a analysis in a eutrophic reservoir using Sentinel-2. Sustainability 13 (15). https://doi.org/10.3390/su13158570.
Vojinovic, Z., Alves, A., Gómez, J.P., Weesakul, S., Keerakamolchai, W., Meesuk, V., Sanchez, A., 2021. Effectiveness of small-and large-scale Nature-Based Solutions for flood mitigation: The case of Ayutthaya, Thailand. Sci. Total Environ. 789, 147725.
Vuolo, F., Neuwirth, M., Immitzer, M., Atzberger, C., Ng, W.-T., 2018. How much does multi-temporal Sentinel-2 data improve crop type classification? Int. J. Appl. Earth Obs. Geoinf. 72, 122–130. https://doi.org/10.1016/j.jag.2018.06.007.
Weigand, M., Staab, J., Wurm, M., Taubenböck, H., 2020. Spatial and semantic effects of LUCAS samples on fully automated land use/land cover classification in high-resolution Sentinel-2 data. Int. J. Appl. Earth Obs. Geoinf. 88, 102065.
Xunta de Galicia, 2021. Meteogalicia. https://www.meteogalicia.gal/Caire/index.action?request_locale=gl.
Xunta de Galicia: Augas de Galicia, 2015. Borrador del Plan de Gestión del Riesgo de Inundación de Galicia Costa 2015/2021. Http://Aae.Medioambiente.Xunta.Es/Aae/VerArquivo.Do;Jsessionid=33C66A862D0571AC53E9FAE7A8DAAF16.Vmprd17?Idd=7491.
Xunta de Galicia: Augas de Galicia, 2021. Avaliación Preliminar do Risco de Inundación.
Zabret, K., Šraj, M., 2015. Can urban trees reduce the impact of climate change on storm runoff? Urbani Izziv 26, S165–S178.
Zhang, K., Chao, L., Wang, Q., Huang, Y., Liu, R., Hong, Y., Tu, Y., Qu, W., Ye, J., 2019. Using multi-satellite microwave remote sensing observations for retrieval of daily surface soil moisture across China. Water Sci. Eng. 12 (2), 85–97.
Zhang, K., Shalehy, M.H., Ezaz, G.T., Chakraborty, A., Mohib, K.M., Liu, L., 2022. An integrated flood risk assessment approach based on coupled hydrological-hydraulic modeling and bottom-up hazard vulnerability analysis. Environ. Model. Softw. 148, 105279 https://doi.org/10.1016/j.envsoft.2021.105279.